Reaction Kinetics, Mechanisms and Catalysis (2023) 136:2123–2145
https://doi.org/10.1007/s11144-023-02439-3

Development of $SO_4^{2-}/ZnAl_2O_4–ZrO_2$ composite solid acids for efficient synthesis of green biofuels via the typical esterification reaction of oleic acid with methanol

Junxia Wang[1] · Anqi Wang[1] · Yu Liao[1] · Li Shi[1] · Lixia Yang[1]

Received: 8 March 2023 / Accepted: 21 June 2023 / Published online: 3 July 2023

Abstract

A novel series of $SO_4^{2-}/ZnAl_2O_4–ZrO_2$ composite solid acids for efficient synthesis of green biodiesel via the typical esterification reaction of oleic acid with methanol were prepared by a simple sol–gel-impregnation method. Their structures and acid properties were studied by means of XRD, FE-SEM, TG, NH_3-TPD, XPS, FT-IR, NH_3 adsorption FT-IR spectra and acid–base titration. The experimental results revealed that the addition of $ZnAl_2O_4$ was successfully achieved to stabilize the active tetragonal phase of ZrO_2 in $SO_4^{2-}/ZnAl_2O_4–ZrO_2$ composite solid acids. Both $ZnAl_2O_4$ and ZrO_2 acted as active components and participated in the formation of active acid center structure for $SO_4^{2-}/ZnAl_2O_4–ZrO_2$ composite solid acids. As a result, the comprehensive acidic properties of $SO_4^{2-}/ZnAl_2O_4–ZrO_2$ composite solid acids were effectively regulated by the mass ratio of $ZnAl_2O_4$ to ZrO_2. Among them, $SO_4^{2-}/ZnAl_2O_4–ZrO_2$ (8:2) exhibited the highest catalytic activity and the better reusability in the esterification reaction of oleic acid with methanol, which might be ascribed to its supreme number of acid sites, its excellent structural stability and its better stability of the surface active sites. The kinetic and thermodynamic analysis demonstrated that $SO_4^{2-}/ZnAl_2O_4–ZrO_2$ (8:2) composite solid acid could effectively catalyze the synthesis of green biodiesel because of its relatively lower values of activation energy in the esterification reaction of oleic acid with methanol. The inevitable loss of sulfate species on the surface of $SO_4^{2-}/ZnAl_2O_4–ZrO_2$ (8:2) might be one of the major reasons for its slight deactivation during acid catalyzed esterification reaction.

Keywords $SO_4^{2-}/ZnAl_2O_4–ZrO_2$ · Composite solid acids · Biodiesel · Esterification reaction · Acid catalysis

✉ Junxia Wang
wjx76@sina.com

[1] Faculty of Materials Science and Chemistry, China University of Geosciences, Wuhan 430074, China

Introduction

Biodiesel is an environmentally friendly renewable energy that can replace fossil energy because of its non-toxic, sulfur-free, aromatics free, high cetane number and good combustion performance and so on [1–6]. At present, the esterification reaction of fatty acid with alcohol catalyzed by liquid acid catalyst is one of the most commonly used method to synthesize biodiesel in industry. Nevertheless, liquid acid catalyst often had the inevitable problems of recycling difficulty, equipment corrosion, serious equipment corrosion and environmental pollution [7–11]. So, the exploration of substitution environmentally friendly solid acids for liquid acid catalysts to achieve efficient synthesis of green biodiesel has received growing research attention in recent years [12, 13].

SO_4^{2-}/M_xO_y solid acid has been recognized as the most development valuable green catalyst in catalytic esterification synthesis of biodiesel [14–21]. The traditional SO_4^{2-}/M_xO_y solid acid is mainly composed of both active matrix (M_xO_y) and promoter (SO_4^{2-}), which mainly focus on SO_4^{2-}/ZrO_2, SO_4^{2-}/TiO_2 and SO_4^{2-}/SnO_2 systems [22, 23]. Among them, SO_4^{2-}/ZrO_2 has attracted much attention owing to its characteristic advantages of unique strong acid properties, high catalytic activities and good selectivity for catalytic esterification synthesis of biodiesel. Regrettably, the traditional SO_4^{2-}/ZrO_2 still has some scientific problems of restricting its industrial application as follows: On the one hand, the traditional SO_4^{2-}/ZrO_2 solid acid has some shortcomings of fast inactivation, poor stability and short one-way life due to the loss of surface active sulfur and surface area carbon in the catalytic esterification reactions. On the other hand, ZrO_2 crystalline form was easily interconverted between the active tetragonal phase and the inactive monochromic phase during the preparation of SO_4^{2-}/ZrO_2 solid acid [24, 25]. As a result, the traditional SO_4^{2-}/ZrO_2 solid acid inevitably faced with the unstable structure and the poor reusability. In order to resolve the above two scientific problems of the traditional SO_4^{2-}/ZrO_2 solid acid, many researchers have tried to explore the development and application of SO_4^{2-}/ZrO_2–M_xO_y composite solid acids by modified SO_4^{2-}/ZrO_2 with other metallic oxides of M_xO_y [26]. Numerous studies have demonstrated that the addition of other M_xO_y is beneficial to improve the catalytic performance of SO_4^{2-}/ZrO_2–M_xO_y composite solid acids by effective means of optimizing the acid properties or impeding the transition of ZrO_2 from the active tetragonal phase to the inactive monoclinic phase. For example, Xu et al. [27] found that the incorporation of Fe_2O_3 into $Pt/SO_4^{2-}/ZrO_2$ enhanced Brönsted acidity and the catalytic activity for *n*-heptane hydroisomerization. Yu et al. [28] showed that the addition of Yb_2O_3 and Al_2O_3 in SO_4^{2-}/ZrO_2–Yb_2O_3–Al_2O_3 composite solid acids improved the specific surface area and the catalytic activity of the catalyst. Dussadee et al. [29] showed that the addition of 20 wt%La_2O_3 to SO_4^{2-}/ZrO_2 could efficiently promote both esterification and transesterification reactions of palm oil because of its dual strong basic and acid sites. Moreover, the 20 wt%La_2O_3–SO_4^{2-}/ZrO_2 catalyst maintained a relatively stable catalytic behavior. Li et al. [30] found that the appropriate addition of MoO_3 in SO_4^{2-}/ZrO_2–MoO_3 stabilized the metastable-state tetragonal

ZrO_2 crystalloid and inhibited its sintering during the calcination process, which was more efficient to increase the specific surface area and acid content of the catalyst. Fan et al.[31]. showed that the addition of CeO_2 in $S_2O_8^{2-}/ZrO_2$–CeO_2 enhanced its thermal stability of tetragonal ZrO_2 and correspondingly increased its acid strength. It is important to emphasize that the designed synthesis of SO_4^{2-}/ZrO_2–M_xO_y composite solid acids with the thermal stability and superior acid properties remains a challenging subject in recent years. So far, the efficient synthesis of green biofuels over $SO_4^{2-}/ZnAl_2O_4$–ZrO_2 composite solid acids have not yet been extensively reported in relevant literature. Compared with simple oxides of M_xO_y, compound oxide spinel of $ZnAl_2O_4$ has the unique advantage of single crystal shape and the more stable structure. Based on this selection of design ideas, the novel $SO_4^{2-}/ZnAl_2O_4$–ZrO_2 composite solid acids would be expected to obtain the higher structural stability and the superior acid properties.

In this paper, a novel series of $SO_4^{2-}/ZnAl_2O_4$–ZrO_2 composite solid acids were prepared by a simple sol–gel-impregnation method and applied to the typical esterification reaction of oleic acid with methanol for green biodiesel synthesis. The effectively design of $SO_4^{2-}/ZnAl_2O_4$–ZrO_2 composite solid acids were based on the single crystal advantage of $ZnAl_2O_4$ as well as the excellent acid forming capacity of ZrO_2. The structure and acidic properties of $SO_4^{2-}/ZnAl_2O_4$–ZrO_2 composite solid acids were systematically investigated by the means of XRD, FE-SEM, TG, NH_3-TPD, XPS, FT-IR, NH_3 adsorption FT-IR spectra and acid–base titration. Additionally, we investigated the effect of both the calcination temperature and the different mass ratio of $ZnAl_2O_4$ to ZrO_2 on the structures and the comprehensive acidic properties of $SO_4^{2-}/ZnAl_2O_4$–ZrO_2 composite solid acids in detail. In order to further evaluate the comprehensive catalytic performance of the optimal $SO_4^{2-}/ZnAl_2O_4$–ZrO_2 (8:2) composite solid acid for green biodiesel synthesis, we delved into its reusability, its kinetic study and its essential reasons for its high stability and its slight deactivation during the acid catalyzed esterification reaction. As a novel catalyst system for acid catalyzed reaction, $SO_4^{2-}/ZnAl_2O_4$–ZrO_2 composite solid acids have the prominent advantages of easy preparation, high structural stability, excellent acid catalytic activity and reuse stability, environmentally friendly and so on.

Experimental

Catalyst preparation

Preparation of $ZnAl_2O_4$

$ZnAl_2O_4$ spinel oxide was synthesized by sol–gel method. $Al(NO_3)_3{\cdot}9H_2O$ and $Zn(NO_3)_2{\cdot}6H_2O$ with the molar ration of 2:1 were dissolved in ethanol. Then, PEG-2000 (5 wt% of the total mass of nitrates) was added to the above solution and keep stirring for 4 h at room temperature. The obtained mixture solution was evaporated at 65 °C for 1 h to obtain the sol. The sol was dried at 120 °C to become a dried gel.

The dried gel was grounded into a fine powder and was calcined at 600 °C for 5 h in air to obtain $ZnAl_2O_4$ spinel oxide.

Preparation of $ZnAl_2O_4$–ZrO_2

According to the certain mass ratio of $ZnAl_2O_4$ to the ZrO_2, the above obtained fine $ZnAl_2O_4$ powder was dispersed in $ZrOCl_2{\cdot}8H_2O$ aqueous solution with constant stirring. Then, aqueous ammonia was added to form the precipitate under pH of 8 ~ 9. The precipitate was aged for one day at room temperature. Afterwards, the precipitate was washed with distilled water to completely remove the chloride ions. At last, the precipitate was filtered and dried at 100 °C to obtain $ZnAl_2O_4$–ZrO_2 composite active matrix. The composite active matrix with the mass ratio of $ZnAl_2O_4$ to ZrO_2 of 1:0, 8:2, 6:4, 4:6 2:8 and 0:1, which were correspondingly designated as $ZnAl_2O_4$, $ZnAl_2O_4$–ZrO_2 (8:2), $ZnAl_2O_4$–ZrO_2 (6:4), $ZnAl_2O_4$–ZrO_2 (4:6), $ZnAl_2O_4$–ZrO_2 (2:8) and ZrO_2.

Preparation of SO_4^{2-}/$ZnAl_2O_4$–ZrO_2 composite solid acids

A portion of $ZnAl_2O_4$–ZrO_2 composite active matrix were impregnated with a certain volume (1 g/10 mL) of 1.5 M $(NH_4)_2SO_4$ (ammonium sulfate) and stirred for 4 h. After filtration, the above sample was dried at 100 °C and calcined for 3 h at 600 °C to obtain SO_4^{2-}/$ZnAl_2O_4$–ZrO_2 composite solid acids, which were denoted as SO_4^{2-}/$ZnAl_2O_4$, SO_4^{2-}/$ZnAl_2O_4$–ZrO_2 (8:2), SO_4^{2-}/$ZnAl_2O_4$–ZrO_2 (6:4), SO_4^{2-}/$ZnAl_2O_4$–ZrO_2 (4:6), SO_4^{2-}/$ZnAl_2O_4$–ZrO_2 (2:8) and SO_4^{2-}/ZrO_2.

Catalyst characterization

The structural characterization was completed by X-ray powder diffraction (XRD) performed on Bruker AXS D8-Focus. XRD were recorded in the range of $2\theta = 10$–70°. Field emission scanning electron microscopy (FE-SEM) measurements were performed on S4800. The dried samples were coated with gold. Thermogravimetric analysis (TG) were performed on a STA-409PC thermoanalyzer in the temperature range of 50~1000 °C with a heating rate of 10 °C min^{-1}. NH_3 Temperature Programmed Desorption (NH_3-TPD) experiment was carried out using a TP-5076 TPD/TPR. X-ray photoelectron spectroscopy (XPS) was performed on a VG Multilab 2000. The Fourier transform Infrared Spectroscopy (FT-IR) spectra was recorded by a Nicolet 6700 IR spectrometer in the range of 400–4000 cm^{-1} and coupled with KBr pellet technique. KBr was pretreated by drying for 4 h at 100 °C before using and was ground to a powder under the infrared lamp. Then, the samples and KBr were mixed and pressed into pellet on a hydraulic tablet machine. The final FT-IR spectra of the sample was obtained by eliminating the background spectrum. The sample examined by FT-IR coupled with NH_3 chemisorption was pre-treated in a He flow (20 mL min^{-1}) at 300 °C for 1 h. Then, the dried sample as cooled to 60 °C and exposed to NH_3 (20 mL min^{-1}) at room temperature for 1 h, and followed by heated up to 120 °C and flowed by helium (20 mL min^{-1}) for 1 h to remove gas-phase and

physically adsorbed NH_3. The obtained samples were examined by FT-IR by using KBr technique, which obtained the FT-IR of NH_3 chemisorption. The shown spectra were obtained after normalized and subtracted by the FT-IR of samples without chemisorption of NH_3. The acid site density of catalysts was determined by ion-exchange titration. 100 mg of the catalyst was added to 25 mL of 0.1 mol L^{-1} NaCl solution and stirred for 24 h at room temperature. The catalyst was separated by filtration. The filtrate was titrated by 0.10 mol L^{-1} NaOH solution using phenolphthalein as an indicator to obtain the corresponding acid values. The total acid densities of the catalysts were estimated by the acid values [32].

Catalytic activity test

The esterification reaction of oleic acid with methanol was tested in a three-necked round flask equipped with a magnetic stirrer, a thermometer and a refluxing condenser tube. The conditions of esterification reaction were as follows: the reaction temperature was 65 °C; the molar ratio of oleic acid to methanol was 1:25; the reaction time was 8 h, the amount of catalysts was 5 wt% (based on the mass of oleic acid). According to the references [33, 34] and the method of GB1668-81, the acid–base titration had been used to calculate the conversion of oleic acid on the basis of acid value. The detailed process was as follows: the 0.50 mL initial reaction mixture or the 0.50 mL final reaction mixture were diluted in 20.00 mL ethanol. Then, the diluted mixtures were titrated by 0.10 mol L^{-1} NaOH solution with an indicator of phenolphthalein. The conversion of oleic acid could be calculated from Eq. 1:

$$\text{Conversion of acetic acid}(\%) = \frac{M_0 - M_1}{M_0} \times 100 \quad (1)$$

Here M_0 represented the volume of NaOH consumed by the initial reaction mixture and M_1 represented the volume of NaOH consumed by final reaction mixture.

In order to evaluate the reusability, the optimal $SO_4^{2-}/ZnAl_2O_4–ZrO_2$ (8:2) composite solid acid after finishing each catalytic evaluation was repeatedly used for the next new esterification reaction of oleic acid with methanol only through filtering and drying.

Results and discussion

Characterization

It is well known that the crystal structure of SO_4^{2-}/M_xO_y solid acid is closely related to its acidity and its catalytic activity. Based on this consideration, we explored the influence of the calcination temperature on the crystal structure of SO_4^{2-}/ZrO_2 and $SO_4^{2-}/ZnAl_2O_4–ZrO_2$ (4:6). As shown in Fig. 1, only a weak peak of active tetragonal phase ZrO_2 at $2\theta = 30.4°$ was observed in SO_4^{2-}/ZrO_2 at the lower calcination temperature of 500 °C [35]. The characteristic diffraction peaks of ZrO_2

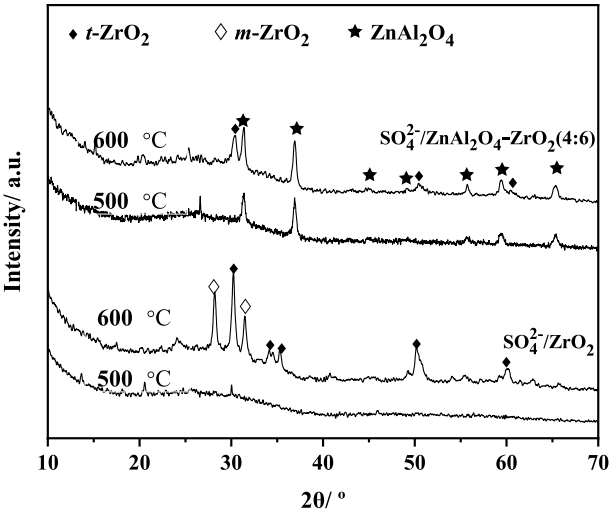

Fig. 1 XRD patterns of SO_4^{2-}/ZrO_2 and $SO_4^{2-}/ZnAl_2O_4–ZrO_2$ (4:6) solid acids at the different calcination temperatures of 500 °C and 600 °C. (Operating conditions: Operating voltage: 40 kV, Scan range: 10°–70°, Scan speed: 10° min^{-1}, Cu target)

active tetragonal phase became very obvious in SO_4^{2-}/ZrO_2 at the higher calcination temperature of 600 °C. Regrettably, the inactive monoclinic phase of ZrO_2 at 2θ of 28.2° and 31.5° was also generated in SO_4^{2-}/ZrO_2 at the higher calcination temperature of 600 °C. This above result demonstrated that the higher calcination temperature resulted in the transformation of ZrO_2 crystal form between the active tetragonal phase and the inactive monochromic phase, which would affect the activity of SO_4^{2-}/ZrO_2 solid acid [36]. It was worth emphasizing that the calcination temperatures had no evident influence on compound oxide spinel of $ZnAl_2O_4$ in $SO_4^{2-}/ZnAl_2O_4–ZrO_2$ (4:6). As shown in Fig. 1, the characteristic diffraction peaks of $ZnAl_2O_4$ spinel at 2θ of 31.5°, 37.1°, 45.1°, 49.3°, 55.9°, 59.6° and 65.5° (JCPDS No.05–0669) were all observed in $SO_4^{2-}/ZnAl_2O_4–ZrO_2$ (4:6) composite solid acid at the different calcination temperatures of 500 and 600 °C. Surprisingly, the diffraction peaks of ZrO_2 monoclinic phase were almost undetected in $SO_4^{2-}/ZnAl_2O_4–ZrO_2$ (4:6). As expected, the transformation of ZrO_2 from active tetrahedron to inactive monoclinic was successfully inhibited by the addition of $ZnAl_2O_4$ in $SO_4^{2-}/ZnAl_2O_4–ZrO_2$ (4:6) at the higher calcination temperatures of 600 °C. As a result, the better structural stability might be more beneficial to improve the reusability $SO_4^{2-}/ZnAl_2O_4–ZrO_2$ composite solid acid by compared with SO_4^{2-}/ZrO_2.

On the basis of experimental results in Fig. 2, we further investigated the effect of the mass ratios of $ZnAl_2O_4$ to ZrO_2 on the crystal structure of $SO_4^{2-}/ZnAl_2O_4–ZrO_2$ composite solid acids at the calcination temperature of 600 °C. As shown in Fig. 2, the characteristic diffraction peaks of $ZnAl_2O_4$ spinel were still evident in both $SO_4^{2-}/ZnAl_2O_4$ and $SO_4^{2-}/ZnAl_2O_4–ZrO_2$ composite solid acids owing to its single crystal shape and its stable structure. On the contrary, the mass ratios of $ZnAl_2O_4$ to ZrO_2 had the obvious influence on the crystal structure of ZrO_2. Both active

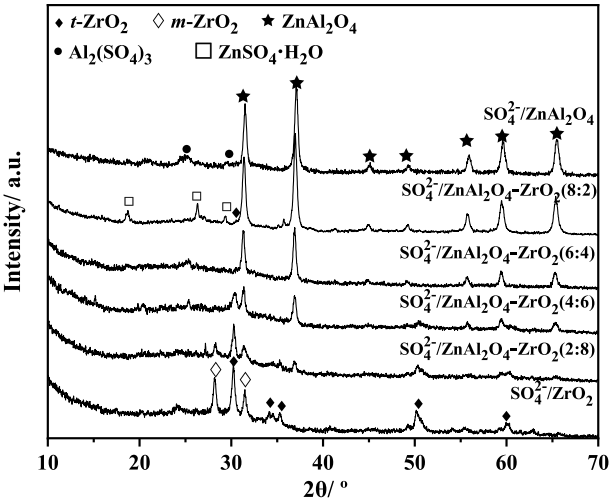

Fig. 2 XRD patterns of $SO_4^{2-}/ZnAl_2O_4$–ZrO_2 composite solid acids with the different mass ratios of $ZnAl_2O_4$ to ZrO_2 at the calcination temperature of 600 °C. (Operating conditions: Operating voltage: 40 kV, Scan range: 10°–70°, Scan speed: 10° min^{-1}, Cu target)

tetragonal ZrO_2 and inactive monoclinic ZrO_2 coexisted in SO_4^{2-}/ZrO_2 and $SO_4^{2-}/ZnAl_2O_4$–ZrO_2 (2:8). However, it could be clearly observed that the diffraction peaks of inactive monoclinic ZrO_2 were gradually reduced with increasing the mass ratio of $ZnAl_2O_4$ to ZrO_2 in $SO_4^{2-}/ZnAl_2O_4$–ZrO_2 composite solid acids. Finally, the distinct inactive monoclinic phase almost disappeared and the active tetragonal ZrO_2 still presented in $SO_4^{2-}/ZnAl_2O_4$–ZrO_2 (4:6) [35]. This above results further proved that the addition of $ZnAl_2O_4$ could effectively retard the crystal transformation of ZrO_2 from the active tetragonal phase to the inactive monoclinic phase, which was in good agreement with the results of Fig. 1. As shown in Fig. 2, the characteristic diffraction peaks of $ZnAl_2O_4$ spinel became stronger and the characteristic diffraction peaks of ZrO_2 tetragonal phase gradually became weaker with increasing the mass ratio of $ZnAl_2O_4$ to ZrO_2. At last, the characteristic diffraction peaks of ZrO_2 tetragonal phase almost disappeared in $SO_4^{2-}/ZnAl_2O_4$–ZrO_2 (6:4) and $SO_4^{2-}/ZnAl_2O_4$–ZrO_2 (8:2). The possible reasons for this result might be that both $ZnAl_2O_4$ and ZrO_2 were well incorporated in the crystal lattice of $SO_4^{2-}/ZnAl_2O_4$–ZrO_2. On the other hand, ZrO_2 might be covered with the surface of $ZnAl_2O_4$ in $SO_4^{2-}/ZnAl_2O_4$–ZrO_2 according to SEM results. Combining with the results of Figs. 1 and 2, we could draw an important conclusion that both the calcination temperature and the mass ratios of $ZnAl_2O_4$ to ZrO_2 had a critical effect on the crystal structure of $SO_4^{2-}/ZnAl_2O_4$–ZrO_2 composite solid acids, which might be one of the essential reasons for their different acidic properties and their different catalytic activities. Therefore, the appropriate calcination temperature and the optimum mass ratio of $ZnAl_2O_4$ to ZrO_2 were beneficial to successfully form the high performance solid acids. Besides, some weak peaks of $Al_2(SO_4)_3$ and $ZnSO_4{\cdot}H_2O$ were observed in some samples because of the long-time impregnation and the interaction between

excess SO_4^{2-} and the metal ions, which might be ineffective for the catalytic activity [37].

SEM was performed to observe the surface morphology of $SO_4^{2-}/ZnAl_2O_4$, $SO_4^{2-}/ZnAl_2O_4$–ZrO_2 (8:2) and SO_4^{2-}/ZrO_2. As shown in Figs. S1a and S1b, $SO_4^{2-}/ZnAl_2O_4$ exhibited the typically sphere-like nanoparticles (~ 50 nm) and the nanoparticles assembled together. However, SO_4^{2-}/ZrO_2 showed the lager bulk morphology and its surface was very smooth in Figs. S1e and S1f. As shown in Figs. S1c and S1d, it was clearly observed that $SO_4^{2-}/ZnAl_2O_4$–ZrO_2 (8:2) composite solid acid performed the similar bulk morphologies with SO_4^{2-}/ZrO_2. In the meantime, the sphere-like $ZnAl_2O_4$ were highly dispersed on the surface of ZrO_2 bulk. This result further demonstrated that both $ZnAl_2O_4$ and ZrO_2 were successfully composited in $SO_4^{2-}/ZnAl_2O_4$–ZrO_2 (8:2), which was in good accordance with the result of XRD. Especially, $SO_4^{2-}/ZnAl_2O_4$–ZrO_2 (8:2) composite solid acid still kept the advantageous structures of ZrO_2. Moreover, ZrO_2 inhibited the aggregation of $ZnAl_2O_4$ particles and facilitated the dispersion of $ZnAl_2O_4$ on the surface of $SO_4^{2-}/ZnAl_2O_4$–ZrO_2 (8:2) composite solid acid. According to Figs. S1a, S1c and S1e, it could be found that the morphology of $SO_4^{2-}/ZnAl_2O_4$–ZrO_2 (8:2) relatively became the loosest among these catalysts, which was advantageous for heterogeneous reactions.

It is well known that the active acid center of SO_4^{2-}/M_xO_y solid acid comes from the coordination adsorption of SO_4^{2-} with the surface metal ions of M_xO_y. Correspondingly, the characteristic absorption peak associated with acid center structure will appear in FT-IR spectra. Based on this consideration, Fig. 3 shows the FT-IR

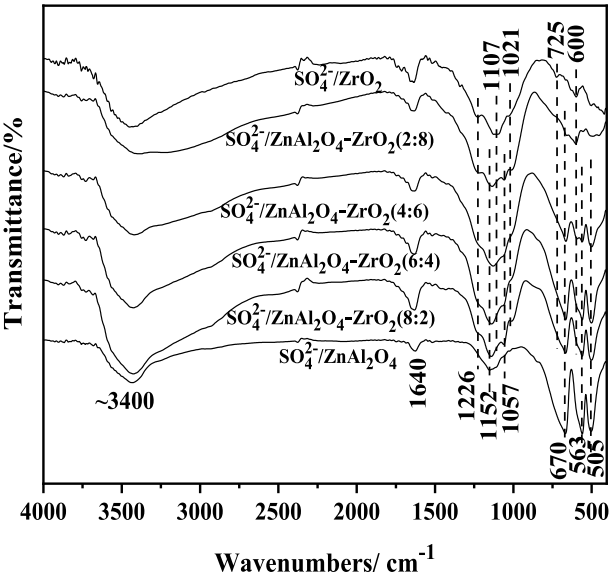

Fig. 3 FT-IR spectra of SO_4^{-}/ $ZnAl_2O_4$–ZrO_2 composite solid acids with the different mass ratios of $ZnAl_2O_4$ to ZrO_2. (Experiment conditions: the calcination temperature of 600 °C; Operating conditions: Scan range: 400–4000 cm^{-1}, KBr pellet)

spectra of $SO_4^{2-}/ZnAl_2O_4$, SO_4^{2-}/ZrO_2 and $SO_4^{2-}/ZnAl_2O_4$–ZrO_2 composite solid acids with the different mass ratios $ZnAl_2O_4$ to ZrO_2. The specific bands in the range of 900 and 1400 cm^{-1} for all the samples were formed by corresponding to their active acid structures on the surface of the samples, which was attribute to the strong interaction between the sulfuric groups and the metal ions [38]. The formation of the active acid center structure was the essential reason for their certain acid catalytic activities of the samples. Among them, the band at ~ 1226 cm^{-1} due to the stretching vibration of S=O was detected in all samples, indicating that a chelating bidentate structure was formed between the surface sulfate species and the metal ions [39, 40]. Such a bidentate structure is believed to be a driving force in the generation of many acidic sites on the surface of SO_4^{2-}/M_xO_y solid acids, making the samples possess super acidity. Additionally, two bands at 1057 and 1152 cm^{-1} in $SO_4^{2-}/ZnAl_2O_4$ were assigned to the symmetric and asymmetric stretching vibration of S–O, respectively. Nevertheless, these two bands were shifted to 1021 and 1107 cm^{-1} for SO_4^{2-}/ZrO_2, which might be owing to their different linked M–O species in $SO_4^{2-}/ZnAl_2O_4$ and SO_4^{2-}/ZrO_2 [40, 41]. These above relevant bands attributed to the symmetric and asymmetric stretching vibration of S–O were all maintained in $SO_4^{2-}/ZnAl_2O_4$–ZrO_2 composite solid acids, demonstrating that both $ZnAl_2O_4$ and ZrO_2 belonged to their active component and were involved in their formation of acid centers. It was important to note that the synergistic promotion between $ZnAl_2O_4$ and ZrO_2 might benefit to adjust the comprehensive acidities of $SO_4^{2-}/ZnAl_2O_4$–ZrO_2 composite solid acids, which was also proved by the following experimental results of NH_3-TPD and NH_3 adsorption FT-IR spectra. In addition, the distinct bands at 505, 563 and 670 cm^{-1} ascribed to Zn–O–Al, Al-O and Zn–O vibrations for $ZnAl_2O_4$ spinel were observed in $SO_4^{2-}/ZnAl_2O_4$ and $SO_4^{2-}/ZnAl_2O_4$–ZrO_2 composite solid acids, which was in good agreement with the XRD results [42, 43]. Two bands at 600 cm^{-1} and 725 cm^{-1} ascribed to Zr–O stretching vibrations were detected in SO_4^{2-}/ZrO_2 and partial $SO_4^{2-}/ZnAl_2O_4$–ZrO_2 [44, 45], which were well in agreement with the XRD analysis. Besides, the bands located at 1640 cm^{-1} and 3400 cm^{-1} resulted from the bending and stretching mode of the OH group of water molecules, respectively.

It was generally accepted that the surface acidic types of SO_4^{2-}/M_xO_y solid acids were significant to their acid catalytic performances [46, 47]. NH_3 is frequently used as the probe molecule in the FT-IR spectra to distinguish the Brönsted acid sites from the Lewis acid sites by the means of NH_3 adsorption FT-IR spectra. NH_3 interacts with the Brönsted acid sites to generate surface NH_4^{+}* and the asymmetric bending vibration of surface NH_4^{+*} will appear at ~ 1400 cm^{-1} in NH_3 adsorption FT-IR spectra. The lone pair electrons on NH_3 is coordinated with the Lewis acid sites to form NH_3* and the symmetric bending vibrations of surface NH_3^{*} will be shown at ~ 1115 cm^{-1} in NH_3 adsorption FT-IR spectra [48, 49]. As shown in the NH_3 adsorption FT-IR spectra of Fig. 4, it was obviously observed that the strong bands at 1400 and 1115 cm^{-1} were all detected in $SO_4^{2-}/ZnAl_2O_4$, SO_4^{2-}/ZrO_2, $SO_4^{2-}/ZnAl_2O_4$–ZrO_2 (2:8) and $SO_4^{2-}/ZnAl_2O_4$–ZrO_2 (8:2), indicating that both Brønsted acid sites and Lewis acid sites coexisted on the surfaces of the samples. In terms of SO_4^{2-}/ZrO_2, the relative strength of Brønsted acid sites was greater than that of Lewis acid sites. For $SO_4^{2-}/ZnAl_2O_4$, the relative strength of

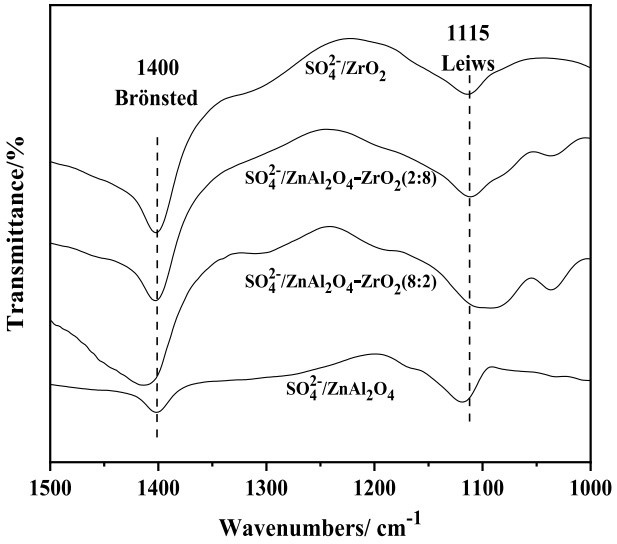

Fig. 4 The NH_3 adsorption FT-IR spectra of SO_4^{2-}/ZrO_2, $SO_4^{2-}/ZnAl_2O_4$ and $SO_4^{2-}/ZnAl_2O_4$–ZrO_2 solid acids. (Conditions: The sample was pre-treated in a He flow of 20 mL min^{-1} at 300 °C for 1 h. Then the dried sample as cooled to 60 °C and exposed to NH_3 of 20 mL min^{-1} at room temperature for 1 h, and followed by heated up to 120 °C and flowed by helium of 20 mL·min^{-1} for 1 h to remove gas-phase and physically adsorbed NH_3. Operating conditions: Scan range: 1000–1500 cm^{-1}, KBr pellet)

Lewis acid sites was greater than that of Brønsted acid sites. It should be emphasized that the combination of $ZnAl_2O_4$ with ZrO_2 was obviously good for regulating the ratio of Brønsted/Lewis acid sites in $SO_4^{2-}/ZnAl_2O_4$–ZrO_2. Among the samples, $SO_4^{2-}/ZnAl_2O_4$–ZrO_2 (8:2) showed the highest mass ratio Brønsted/Lewis acid sites and the most number of acid sites, which might be one of the essential reasons for its higher catalytic activity in acid catalyzed esterification of oleic acid with methanol. This result was manifested that the combination of $ZnAl_2O_4$ and ZrO_2 might be more beneficial to adjust the acid type by compared with the traditional SO_4^{2-}/ZrO_2 solid acid.

The acid strength distribution obtained from the NH_3-TPD of $SO_4^{2-}/ZnAl_2O_4$, $SO_4^{2-}/ZnAl_2O_4$–ZrO_2 (8:2) and SO_4^{2-}/ZrO_2 solid acids are shown in Fig. 5. Generally, the desorption temperature was closely related to the acid strength. The higher the desorption peak temperatures was, the stronger the acid strength was [50]. Meanwhile, the area of the desorption peak corresponded to the number of active acid centers. The bigger the area was, the more active acid centers were. According to the desorption temperature, the acid strength was divided into the weak (120 ~ 250 °C), the medium (250 ~ 400 °C) and the strong (> 400 °C) strength. As shown in Fig. 5, $SO_4^{2-}/ZnAl_2O_4$–ZrO_2 (8:2) showed the prominent broad desorption peaks in the range of 120 to 475 °C, which suggested the presence of the weak, the moderate and the strong acidic sites. According to Fig. 5, there were some weak acid sites and medium acid sites on the surface of $SO_4^{2-}/ZnAl_2O_4$. However, there were only the strong acid sites on the surface of SO_4^{2-}/ZrO_2. In the meantime, the acid site density of these samples was further studied

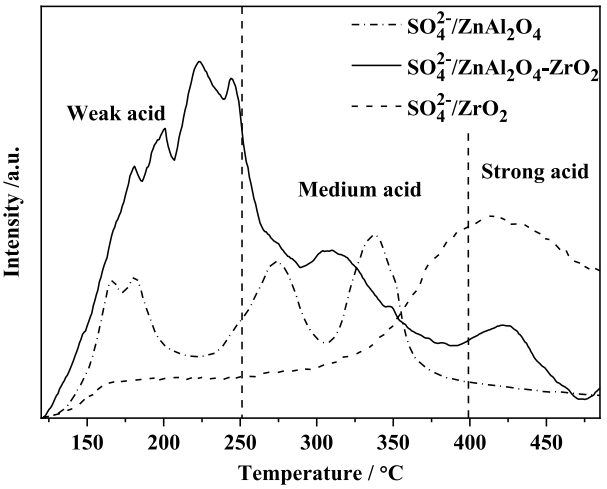

Fig. 5 NH_3-TPD profiles of $SO_4^{2-}/ZnAl_2O_4$, $SO_4^{2-}/ZnAl_2O_4$–ZrO_2 (8:2) and SO_4^{2-}/ZrO_2 solid acids. (Conditions: The sample was pretreated in a He flow of 20 mL min^{-1} at 300 °C for 1 h. Then the dried sample as cooled to 60 °C and exposed to NH_3 of 20 mL min^{-1} at room temperature for 1 h, and followed by heated up to 120 °C and flowed by helium of 20 mL min^{-1} for 1 h to remove gas-phase and physically adsorbed NH_3. After removing the physically adsorbed NH_3, measurements were started in helium flow of 20 mL·min^{-1} with a heating rate of 10 °C min^{-1})

Table 1 The acid site density of SO_4^{2-}/ZrO_2, $SO_4^{2-}/ZnAl_2O_4$ and $SO_4^{2-}/ZnAl_2O_4$–ZrO_2

Catalysts	Acid sites (mmol g^{-1})
$SO_4^{2-}/ZnAl_2O_4$	1.12
$SO_4^{2-}/ZnAl_2O_4$–ZrO_2(8:2)	2.45
$SO_4^{2-}/ZnAl_2O_4$–ZrO_2(6:4)	1.88
$SO_4^{2-}/ZnAl_2O_4$–ZrO_2(4:6)	1.61
$SO_4^{2-}/ZnAl_2O_4$–ZrO_2(2:8)	1.57
SO_4^{2-}/ZrO_2	1.64
$SO_4^{2-}/ZnAl_2O_4$–ZrO_2(8:2)-used	1.47

(Conditions: 100 mg of the catalyst was added to 25 mL of 0.1 mol L^{-1} NaCl solution and stirred for 24 h at room temperature. The catalyst was separated by filtration. The filtrate was titrated by 0.10 mol L^{-1} NaOH solution using phenolphthalein as an indicator.)

by the acid–base titration (shown in Table 1). Among them, $SO_4^{2-}/ZnAl_2O_4$ showed the lowest acid site density. As shown in Table 1, it was worth mentioning that the mass ratio of $ZnAl_2O_4$ to ZrO_2 had a significant effect on the acid site density. $SO_4^{2-}/ZnAl_2O_4$–ZrO_2 (8:2) had the highest density of acid sites, which might be related to the better dispersion of two components and the synergy between two components of $ZnAl_2O_4$ and ZrO_2 [51]. These above results further demonstrated that both $ZnAl_2O_4$ and ZrO_2 in $SO_4^{2-}/ZnAl_2O_4$–ZrO_2 were active

components and participated in the formation of active acid centers. So, it might be an effective method to regulate the synthetic acid properties and the catalytic activities by additions of $ZnAl_2O_4$ to ZrO_2 in $SO_4^{2-}/ZnAl_2O_4–ZrO_2$, which were also in good consistent with the results of NH_3 adsorption FT-IR. However, the excess ZrO_2 had a negative influence on the acid site density. The acid site density of $SO_4^{2-}/ZnAl_2O_4–ZrO_2$ decreased with increasing the mass ratio of ZrO_2 to $ZnAl_2O_4$. $SO_4^{2-}/ZnAl_2O_4–ZrO_2$ (4:6) and $SO_4^{2-}/ZnAl_2O_4–ZrO_2$ (2:8) revealed the little lower acid site density by compared with SO_4^{2-}/ZrO_2. Combining the results of Figs. 3, 4, 5 and Table 1, we could draw an important conclusion that the suitable mass ratio of ZrO_2 to $ZnAl_2O_4$ played a key role in the comprehensive acidic properties of $SO_4^{2-}/ZnAl_2O_4–ZrO_2$ composite solid acids, which was also reported in other $SO_4^{2-}/ZrO_2–M_xO_y$ composite solid acids [52].

Figs. 6 and 7 give the TG analysis of $SO_4^{2-}/ZnAl_2O_4–ZrO_2$ (8:2) and SO_4^{2-}/ZrO_2, which was used to compare their thermostability. The first weight loss below 200 °C could be assigned to the removal of the physically adsorbed water. The second weight loss in the following temperature range of 200–500 °C was related to the removal of the structure water. The third weight loss at the higher temperature range between 500 and 1000 °C was due to the gradual decomposition of the sulfur species on the surface of the samples [53]. So, the third weight loss above 500 °C was used to estimate the sulfur content and the amounts of the acid sites on the surface of the samples. Accordingly, the more the weight lost, the more the sulfate groups existed. As shown in Fig. 6, $SO_4^{2-}/ZnAl_2O_4–ZrO_2$ (8:2) gave the mass weight loss of 32.8% above 500 °C. By contrast, SO_4^{2-}/ZrO_2 had the relatively little weight loss of 26.5% above 500 °C (as shown in Fig. 7). This above result revealed that the cooperation of $ZnAl_2O_4$ and ZrO_2 was beneficial to improve the number of acid center and the surface resistance to sulfur loss. As a result, $SO_4^{2-}/ZnAl_2O_4–ZrO_2$ (8:2) had the higher catalytic activity.

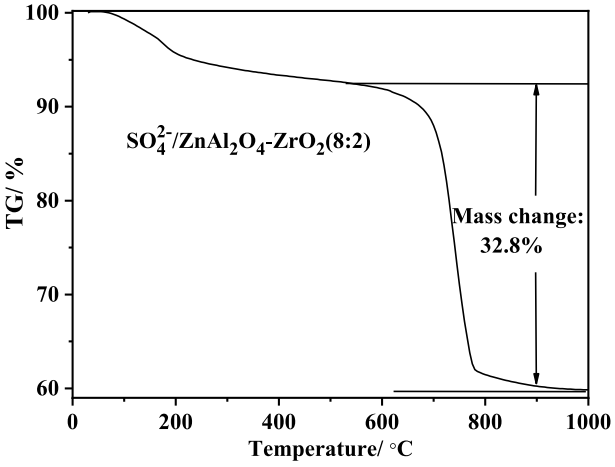

Fig. 6 TG curves of $SO_4^{2-}/ZnAl_2O_4–ZrO_2$ (8:2). (Operating conditions: Scan range: from room temperature to 1000 °C, Heating rate: 20 °C min^{-1})

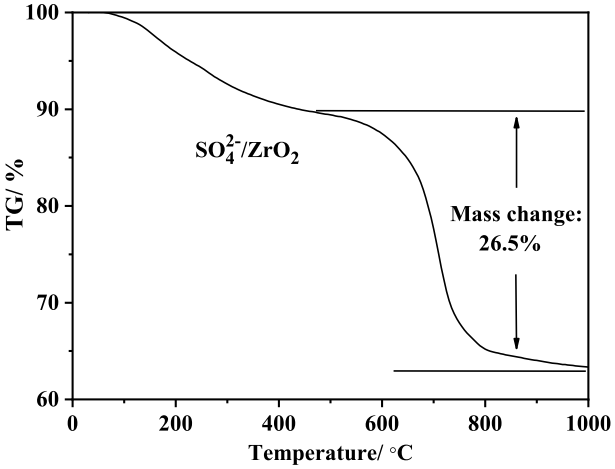

Fig. 7 TG curves of SO_4^{2-}/ZrO_2. (Conditions: Scan range: from room temperature to 1000 °C, Heating rate: 20 °C min^{-1})

The surface composition and the oxidation state of $SO_4^{2-}/ZnAl_2O_4–ZrO_2$ (8:2) composite solid acid were further investigated by the means of XPS. As shown in Fig. S2, Zn, Zr, Al, O, S and C elements were all detected in $SO_4^{2-}/ZnAl_2O_4–ZrO_2$ (8:2). The observed peak of C 1s might originate from the signal carbon in the instrument and was used for the calibration. The broad O1s peak was consisted of three distinct peaks at 530.1, 531.5 and 532.5 eV, which were ascribed to the lattice oxygen of the oxides contribution, the oxygen of OH species and the sulfate oxygen, [54].The Zn 2p3/2 and Zn 2p1/2 binding energies were located at 1021.5 eV and 1044.8 eV, which were close to the standard data for Zn^{2+}. Fig. S2e shows the Al 2p peak of the catalyst at 75.3 eV, which was assigned to the Al^{3+} ion [55]. The peaks at 183.5 eV and 185.9 eV correspond to Zr $3d_{5/2}$ and Zr $3d_{3/2}$, respectively, indicating that Zr species existed as the formation of Zr(IV) [56]. With reference to the XRD result, the intensity of ZrO_2 diffraction peaks became no apparent in $SO_4^{2-}/ZnAl_2O_4–ZrO_2$ (8:2). So, the detection of the Zr in XPS further evidenced that ZrO_2 might be highly dispersed on the surface of the sample. Additionally, it was necessary to emphasize that the peak at 169.5 eV corresponding to S 2p binding energy was clearly observed in $SO_4^{2-}/ZnAl_2O_4–ZrO_2$ (8:2), which was attributable to the sulfur oxidation state of + 6 [57]. It is well known that S^{6+} contributes to the formation of the surface acid sites. The suction-induced complex S=O promotes the electron-accepting ability for the metal atoms, making the sample possess supper acid. Accordingly, IR spectra of $SO_4^{2-}/ZnAl_2O_4–ZrO_2$ (8:2) showed the special bands of the active acid structures in the range of 900–1400 cm^{-1}. XPS analysis further confirmed that the surface active sulfur species, $ZnAl_2O_4$ and ZrO_2 coexisted in $SO_4^{2-}/ZnAl_2O_4–ZrO_2$ (8:2) composite solid acid.

Catalytic activities

According to XRD results, the mass ratios of $ZnAl_2O_4$ to ZrO_2 had a key influence on the crystal structure of $SO_4^{2-}/ZnAl_2O_4–ZrO_2$ composite solid acids, which is a very critical factor to affect their acid catalytic performance. Based on this consideration, the catalytic activities of $SO_4^{2-}/ZnAl_2O_4–ZrO_2$ composite solid acids with the different mass ratios of $ZnAl_2O_4$ to ZrO_2 in the esterification reaction of oleic acid with methanol were shown in Fig. 8. It was clearly observed that all the samples displayed the certain catalytic activities in esterification reaction of oleic acid with methanol, which resulted from their formation of active acid center structure. Compare with SO_4^{2-}/ZrO_2 and $SO_4^{2-}/ZnAl_2O_4$, the catalytic activities of $SO_4^{2-}/ZnAl_2O_4–ZrO_2$ composite solid acids were effectively modified by combination of $ZnAl_2O_4$ and ZrO_2, which might be owing to their different acidic properties on the basis of the NH_3 adsorption FT-IR spectra, TG, NH_3-TPD and acid–base titration analysis. In view of its optimal synthetic acid properties among the samples, $SO_4^{2-}/ZnAl_2O_4–ZrO_2$ (8:2) exhibited the highest catalytic activities with more than 80% oleic acid conversion in the esterification reaction of oleic acid with methanol. On this basis, the kinetic profile of the esterification reaction over $SO_4^{2-}/ZnAl_2O_4–ZrO_2$ (8:2) composite solid acid at different reaction temperature of 60, 65 and 70 °C was obtained with the different reaction time. As shown in Fig. 9, it was obviously discovered that the conversion of oleic acid was increased with the increase of the reaction temperature, suggesting that the esterification reaction was be assigned to the kinetically

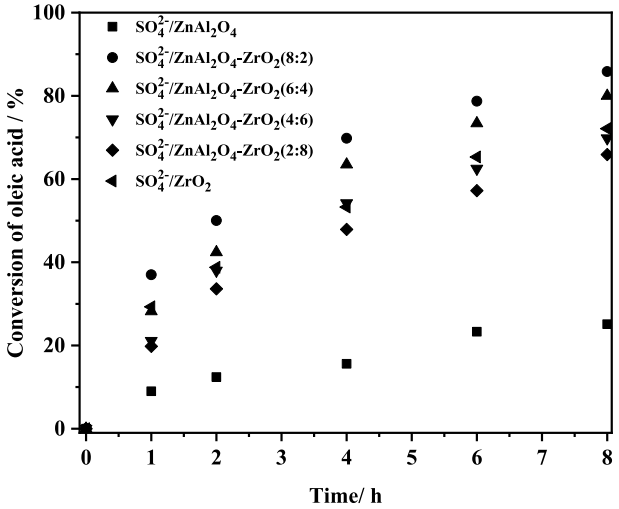

Fig. 8 The catalytic activities of $SO_4^{2-}/ZnAl_2O_4–ZrO_2$ with the different mass ratios of $ZnAl_2O_4$ to ZrO_2 at the calcination temperature of 600 °C. (Reaction conditions: the reaction temperature was 65 °C, the molar ratio of oleic acid to methanol was 1:25, the reaction time was 8 h, the amount of catalysts was 5 wt%)

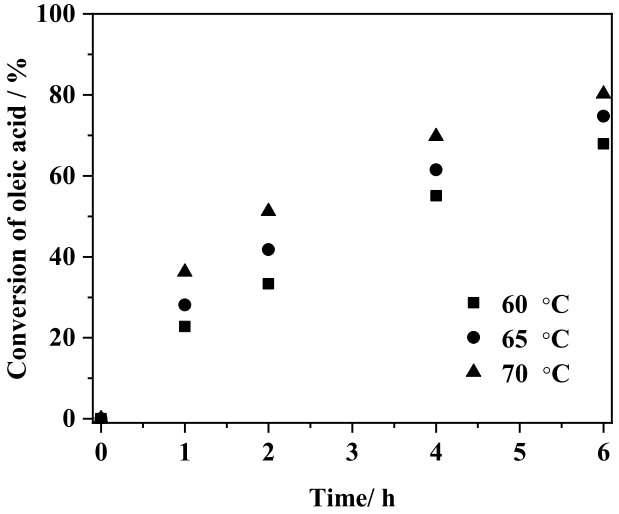

Fig. 9 The catalytic activities of $SO_4^{2-}/ZnAl_2O_4–ZrO_2$ (8:2) at the different reaction temperature. (Reaction conditions: the reaction temperature range was 60–70 °C, the molar ratio of oleic acid to methanol was 1:25, the reaction time was 8 h, the amount of catalysts was 5 wt%)

controlled reaction. Take the boiling point of methanol into account, 65 °C was selected as the optimum temperature for the esterification reaction of oleic acid with methanol.

The esterification reaction of carboxylic acid [A] with alcohol [M] to form esters [E] and water [W] over catalysts is given as Eq. 2:

$$\mathrm{A+M} \overset{K_s}{\Longleftrightarrow} \mathrm{E+W} \tag{2}$$

In order to simplify the kinetic model, the following assumptions were built [28]:

(1) The rate of reaction without catalyst was ignored; (2) The internal and external diffusion effects of matter were ignored; (3) The surface reaction was the rate control step; (4) Both the forward and backward reactions belonged to second-order reactions. The overall rate can be expressed as Eq. 3:

$$r = k_s[\mathrm{A}][\mathrm{M}] - k_{-s}[\mathrm{E}][\mathrm{W}] \tag{3}$$

The k_s represented the rate constant for the forward reaction and the k_{-s} was the rate constant for the reverse reaction.

The following relationship between reactant and product concentrations was followed as Eq. 4:

$$\begin{gathered} n = \frac{[\mathrm{M}]_0}{[\mathrm{A}]_0} \\ [\mathrm{A}] = [\mathrm{A}]_0(1-\mathrm{X}) \quad [\mathrm{M}] = [\mathrm{A}]_0(\mathrm{n}-\mathrm{X}) \\ [\mathrm{E}] = [\mathrm{A}]_0 X \quad [\mathrm{W}] = [\mathrm{A}]_0 X \end{gathered} \tag{4}$$

Symbol n represents the molar ratios of alcohol to carboxylic acid. The X represented the conversion of the acid (< 1). The Eq. 3 can be expressed as in Eq. 5:

$$r = k_s[A]_0^2(1 - X)(n - X) - k_{-s}[A]_0^2X^2 \tag{5}$$

The forward reaction rate was much greater than the reverse reaction rate, so Eq. 5 can be simplified as Eq. 6:

$$r = k_s[A]_0^2(1 - X)(n - X) \tag{6}$$

Equation 6 can be integrated to obtain Eq. 7:

$$\ln\frac{n - X}{n(1 - X)} = [A]_0(n - 1)k_s t \tag{7}$$

Equation (7) was written as Eq. (8) for nonlinear fitting:

$$\frac{n - X}{n(1 - X)} = e^{[A]_0(n-1)k_s t} \tag{8}$$

As shown in Fig. S3, the good nonlinear fitting results indicated that the esterification reaction of oleic acid with methanol conformed to the second order kinetic model. Correspondingly, Table 2 gave the forward rate constants (k_s) at different reaction temperature on the basis of these lines. The activation energy (E_a) could be calculated according to the Arrhenius equation of Eq. (9), which gave the dependence of the forward rate constant on the reaction temperature.

$$-\ln k_s = \frac{E_a}{RT} - \ln A \tag{9}$$

R was the gas constant (8.314 J mol^{-1} K^{-1}), T was the thermodynamic temperature (K), E_a was the activation energy (kJ mol^{-1}) and A was the pre-exponential factor (s^{-1}).

According to the kinetic calculation, the activation energy was 37.5 kJ mol^{-1} for the esterification reaction of oleic acid with methanol, which was the relatively lower than $H_3PW_{12}O_{40}$ and H_2SO_4 (5% and 10%w/w) with the activation energy over 50 kJ mol^{-1} [58]. Combining kinetic study and thermodynamic analysis, these above results strongly demonstrated that $SO_4^{2-}/ZnAl_2O_4–ZrO_2$ (8:2) composite solid acid could effectively catalyze the typical esterification reaction of oleic acid with methanol for the synthesis of green biodiesel.

It is well known that traditional SO_4^{2-}/M_xO_y solid acid can perform the high initial activities. However, they always suffer from rapid deactivation and short lifetime owing to the loss of surface active sulfur, the deposition of surface carbon and the crystal transformation of active carrier. Based on these above considerations, $SO_4^{2-}/ZnAl_2O_4–ZrO_2$ (8:2) composite solid acid was recycled to study its reusability, which is presented in Fig. 10. Compared with SO_4^{2-}/ZrO_2, $SO_4^{2-}/ZnAl_2O_4–ZrO_2$ (8:2) composite solid acid obviously showed the better reusability. The conversion of oleic acid still remained above 75% after being used for four times, suggesting that the synergistic effect of both $ZnAl_2O_4$ and ZrO_2 was

Table 2 Kinetic parameters of esterification reaction

Esterification	Reaction temperature (°C)	k_s (mL mol^{-1} s^{-1})	R^2	Standard errors of k_s (mL mol^{-1} s^{-1})	E_a (kJ mol^{-1})	Standard errors of E_a (kJ mol^{-1})	Reference E_a (kJ mol^{-1})
Oleic acid/methanol	60	0.00867	0.99527	0.00211	37.5	0.01614	50.7 (5% sulphuric acid)[58]
	65	0.01049	0.99315				
	70	0.01287	0.97547				

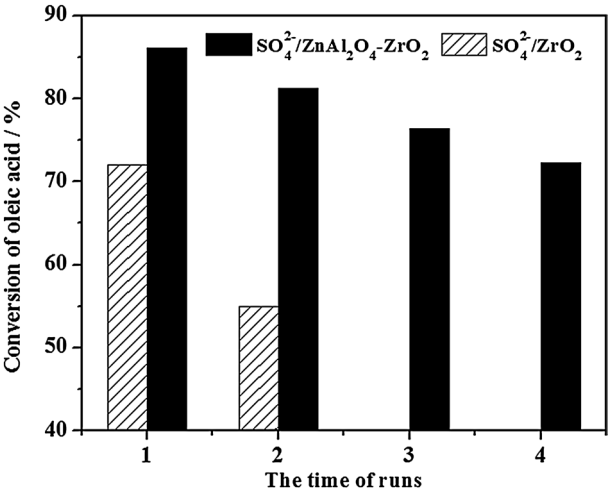

Fig. 10 Reusability of $SO_4^{2-}/ZnAl_2O_4$–ZrO_2 (8:2) and SO_4^{2-}/ZrO_2 for esterification reaction of oleic acid with methanol. (Reaction conditions: the reaction temperature was 65 °C, the molar ratio of oleic acid to methanol was 1:25, the reaction time was 8 h, the amount of catalysts was 5 wt%.The used catalysts were recovered by filtering and drying, after completing each reaction)

beneficial to the improve the reusability of $SO_4^{2-}/ZnAl_2O_4$–ZrO_2 (8:2) composite solid acid.

In order to further explore the essential reasons for its better reusability and its slight deactivation, the fresh and used $SO_4^{2-}/ZnAl_2O_4$–ZrO_2 (8:2) composite solid acid were characterized by means of XRD, TG, direct and NH_3 adsorbed FT-IR. As shown in Figs. S4, S5, S6 and S7, the used $SO_4^{2-}/ZnAl_2O_4$–ZrO_2 (8:2) composite solid acid had no evident changes in the intensity and characteristics peaks in XRD and FT-IR analysis by compared with the fresh catalyst. This above result indicated that used $SO_4^{2-}/ZnAl_2O_4$–ZrO_2 (8:2) still kept its major phase structure, its active acid structures and its acid type on the surface of the sample. As a result, $SO_4^{2-}/ZnAl_2O_4$–ZrO_2 (8:2) showed the better structural stability and the better stability of the surface active sites, which was the essential reason for its higher reusability after recovery process. Additionally, the peaks ascribed to the $ZnSO_4{\cdot}H_2O$ was obviously decreased in the used catalysts and the used catalyst still performed its higher activities, suggesting that $ZnSO_4{\cdot}H_2O$ was not the active component. Moreover, the slight deactivation reason for $SO_4^{2-}/ZnAl_2O_4$–ZrO_2 (8:2) during the acid catalyzed esterification was also deeply investigated in this paper. The used $SO_4^{2-}/ZnAl_2O_4$–ZrO_2 (8:2) had a slight decrease in the intensity of Brønsted and Lewis acid sites bands in NH_3 adsorbed FT-IR spectra, indicating that the number of active acid centers decreased during the acid catalyzed esterification reaction. According to TG analysis, the surface sulfur weight percentages of the fresh and used $SO_4^{2-}/ZnAl_2O_4$–ZrO_2 (8:2) were 32.8% and 21.0%. The comprehensive analysis of TG and Table 1 results certified that the inevitable loss of surface active sulfur species occurred in $SO_4^{2-}/ZnAl_2O_4$–ZrO_2 (8:2), which might be the major reason for its slight deactivation in the process of the acid catalyzed esterification reaction.

Conclusion

A novel series of $SO_4^{2-}/ZnAl_2O_4–ZrO_2$ composite solid acid were successfully used to catalyze the typical esterification reaction of oleic acid with methanol for biodiesel synthesis. The addition of $ZnAl_2O_4$ successfully retarded the crystal transformation of ZrO_2 from the active tetragonal phase to the inactive monoclinic phase. Moreover, both the calcination temperature and the mass ratios of $ZnAl_2O_4$ to ZrO_2 had a critical effect on the crystal structure of $SO_4^{2-}/ZnAl_2O_4–ZrO_2$ composite solid acids, which resulted in their different acidic properties and their different catalytic activities. In the meantime, both $ZnAl_2O_4$ and ZrO_2 acted as active components and participated in the formation of active acid center structure for $SO_4^{2-}/ZnAl_2O_4–ZrO_2$ composite solid acids. As a result, the suitable mass ratio of ZrO_2 to $ZnAl_2O_4$ benefited to adjust the comprehensive acidic properties of $SO_4^{2-}/ZnAl_2O_4–ZrO_2$ composite solid acids, such as the acid type, the acid strength and the number of active acid centers. Among them, the optimal $SO_4^{2-}/ZnAl_2O_4–ZrO_2$ (8:2) composite solid acids exhibited the highest catalytic activities with more than 80% oleic acid conversion in esterification of oleic acid with methanol. Additionally, the kinetic study indicated that $SO_4^{2-}/ZnAl_2O_4–ZrO_2$ (8:2) composite solid acid showed the highly efficient for the esterification of oleic acid with methanol because of its lower activation energy value of 37.5 kJ mol^{-1}. Particularly, the optimal $SO_4^{2-}/ZnAl_2O_4–ZrO_2$ (8:2) had the obviously better reusability with above 75% conversion of oleic acid after being used for four times in the esterification reaction of oleic acid with methanol owing to its excellent structural stability and its better stability of the surface active sites. It was worth mentioning that the used $SO_4^{2-}/ZnAl_2O_4–ZrO_2$ (8:2) had a slight decrease in the intensity of Brønsted and Lewis acid sites bands in NH_3 adsorption FT-IR spectra, indicating that the number of active acid centers decreased during the acid catalyzed esterification reactions. The Further TG result showed that the inevitable loss of sulfate species on the surface of $SO_4^{2-}/ZnAl_2O_4–ZrO_2$ (8:2) resulted in its slight deactivation during the acid catalyzed esterification reaction. The obtained results would provide reference value for designing and synthesizing new composite solid acids with adjustable comprehensive acidities and excellent acid catalytic performance by combination of $ZnAl_2O_4$ with ZrO_2, which might have a broad application prospect in the field of biodiesel synthesis by acid catalyzed esterification reactions.

Supplementary Information The online version contains supplementary material available at https://doi.org/10.1007/s11144-023-02439-3.

Acknowledgements This work was supported by the National Nature Science Foundation of China (No. 2021033144), State Key Laboratory of Inorganic Synthesis and Preparation Chemistry (Jilin University) Open Project (No. 2020-23).

Data availability The authors approve the availability of the data in this publication.

Declarations

Competing interest The authors have no competing interests. All authors have read and agreed to the published version of the manuscript.

References

1. Daud NM, Sheikh Abdullah SR, Abu Hasan H, Yaakob Z (2015) Production of biodiesel and its wastewater treatment technologies: a review. Process Saf Environ 94:487–508. https://doi.org/10.1016/j.psep.2014.10.009
2. Li Y, Zhang XD, Sun L, Xu M, Zhou WG, Liang XH (2010) Solid superacid catalyzed fatty acid methyl esters production from acid oil. Appl Energy 87:2369–2373. https://doi.org/10.1016/j.apenergy.2010.01.017
3. Navas MB, Lick ID, Bolla PA, Casella ML, Ruggera JF (2018) Transesterification of soybean and castor oil with methanol and butanol using heterogeneous basic catalysts to obtain biodiesel. Chem Eng Sci 187:444–454. https://doi.org/10.1016/j.ces.2018.04.068
4. Sronsri C, Sittipol W, U-yen K (2020) Optimization of biodiesel production using magnesium pyrophosphate. Chem Eng Sci 226:115884–115896. https://doi.org/10.1016/j.ces.2020.115884
5. Ye J, Liu C, Fu Y, Peng S, Chang J (2014) Upgrading bio-oil: simultaneous catalytic esterification of acetic acid and alkylation of acetaldehyde. Energ Fule 28:4267–4272. https://doi.org/10.1021/ef500129x
6. Shi WP, Li JW (2013) A new deactivation mechanism of sulfate-promoted iron oxide. Catal Lett 143:1285–1293. https://doi.org/10.1007/s10562-013-1066-7
7. Shu Q, Tang G, Liu F, Zou W, He J, Zhang C, Zou L (2017) Study on the preparation, characterization of a novel solid Lewis acid Al^{3+}-SO_4^{2-}/MWCNTs catalyst and its catalytic performance for the synthesis of biodiesel via esterification reaction of oleic acid and methanol. Fuel 209:290–298. https://doi.org/10.1016/j.fuel.2017.07.113
8. Wang L, Xiao FS (2015) Nanoporous catalysts for biomass conversion. Green Chem 17:24–39. https://doi.org/10.1039/c4gc01622j
9. Huang CC, Yang CJ, Gao PJ, Wang NC, Chen CL, Chang JS (2015) Characterization of an alkaline earth metal-doped solid superacid and its activity for the esterification of oleic acid with methanol. Green Chem 17:3609–3620. https://doi.org/10.1039/c5gc00188a
10. Cheng S, Wei L, Julson J, Muthukumarappan K, Kharel PR (2017) Upgrading pyrolysis bio-oil to hydrocarbon enriched biofuel over bifunctional Fe-Ni/HZSM-5 catalyst in supercritical methanol. Fuel Process Technol 167:117–126. https://doi.org/10.1016/j.fuproc.2017.06.032
11. Mohd Laziz A, KuShaari K, Azeem B, Yusup S, Chin J, Denecke J (2020) Rapid production of biodiesel in a microchannel reactor at room temperature by enhancement of mixing behaviour in methanol phase using volume of fluid model. Chem Eng Sci 219:115532–115542. https://doi.org/10.1016/j.ces.2020.115532
12. Chang BB, Guo YZ, Yin H, Zhang SR, Yang BC (2015) Synthesis of sulfonated porous carbon nanospheres solid acid by a facile chemical activation route. J Solid State Chem 221:384–390. https://doi.org/10.1016/j.jssc.2014.10.029
13. Ravi A, Gurunathan B, Rajendiran N, Varjani S, Gnansounou E, Pandey A, You S, Raman JK, Ramanujam P (2020) Contemporary approaches towards augmentation of distinctive heterogeneous catalyst for sustainable biodiesel production. Environ Technol Inno 19:100906–100924. https://doi.org/10.1016/j.eti.2020.100906
14. Hino M, Kobayashi S, Arata K (1979) Reactions of butane and isobutane catalyzed by zirconium oxide treated with sulfate ion. Solid superacid catalyst. J Am Chem Soc 101:6439–6441. https://doi.org/10.1021/ja00515a051
15. Labidi S, Ben Amar M, Passarello JP, Le Neindre B, Kanaev A (2017) Design of novel sulfated nanozirconia catalyst for biofuel synthesis. Ind Eng Chem Res 56:1394–1403. https://doi.org/10.1021/acs.iecr.6b03448
16. Zane F, Melada S, Signoretto M, Pinna F (2006) Active and recyclable sulphated zirconia catalysts for the acylation of aromatic compounds. Appl Catal A 299:137–144. https://doi.org/10.1016/j.apcata.2005.10.019
17. Li XB, Nagaoka K, Simon LJ, Olindo R, Lercher JA, Hofmann A, Sauer J (2005) Oxidative activation of *n*-butane on sulfated zirconia. J Am Chem Soc 127:16159–16166. https://doi.org/10.1021/ja054126d
18. Xu D, Lai X, Guo W, Zhang X, Wang C, Dai P (2018) Efficient catalytic properties of SO42-/MxOy (M = Cu Co, Fe) catalysts for hydrogen generation by methanolysis of sodium borohydride. Int J Hydrogne Eng 43:6594–6602. https://doi.org/10.1016/j.ijhydene.2018.02.074

19. Vasić K, Hojnik Podrepšek G, Knez Ž, Leitgeb M (2020) Biodiesel production using solid acid catalysts based on metal oxides. Catal 10:237–256. https://doi.org/10.3390/catal10020237
20. Liu XX, Wang K, Liu BQ, Guo ZM, Zhang C, Lv ZG (2021) Novel $WO_3/SO_4^{2-}ZrO_2$-TiO_2 double bridge coordination catalyst hfor oxidation of cyclohexene. J Solid State Chem 300:122239–122246. https://doi.org/10.1016/j.jssc.2021.122239
21. Liu P, Cao J, Xu Z, Yang C, Wang X, Liu F (2020) Thiolation of methanol with H_2S using core-shell structured ZSM-5@t-ZrO_2 catalyst. Chem Eng Sci 211:115273–115282. https://doi.org/10.1016/j.ces.2019.115273
22. Chiang CL, Lin KS, Shu CW, Wu JCS, Wu KCW, Huang YT (2020) Enhancement of biodiesel production via sequential esterification/transesterification over solid superacidic and superbasic catalysts. Catal Today 348:257–269. https://doi.org/10.1016/j.cattod.2019.09.037
23. Ibrahim MM, Mahmoud HR, El-Molla SA (2019) Influence of support on physicochemical properties of ZrO_2 based solid acid heterogeneous catalysts for biodiesel production. Catal Commun 122:10–15. https://doi.org/10.1016/j.catcom.2019.01.008
24. Sohn JR, Lee SH, Lim JS (2006) New solid superacid catalyst prepared by doping ZrO_2 with Ce and modifying with sulfate and its catalytic activity for acid catalysis. Catal Today 116:143–150. https://doi.org/10.1016/j.cattod.2006.01.023
25. Yang H, Zhou Y, Tong D, Yang M, Fang K, Zhou C, Yu W (2020) Catalytic conversion of cellulose to reducing sugars over clay-based solid acid catalyst supported nanosized SO_4^{2-}/ZrO_2. Appl Clay Sci 185:105376–105383. https://doi.org/10.1016/j.clay.2019.105376
26. Li XF, Ma WH, Bao GR, Lv GQ, Wan XH, Li QJ (2021) Effect of preparation parameters on the catalytic performance of solid acid catalyst SO_4^{2-}/ZrO_2-CeO_2 in biodiesel production. Fuel Cells 21:119–125. https://doi.org/10.1002/fuce.202000185
27. Xu X, Liu T, Xie P, Yue Y, Miao C, Hua W, Gao Z (2014) Enhanced catalytic performance over Fe_2O_3-doped Pt/SO_4^{2-}/ZrO_2 in *n*-heptane hydroisomerization. Catal Commun 54:77–80. https://doi.org/10.1016/j.catcom.2014.05.020
28. Yu GX, Zhou XL, Li CL, Chen LF, Wang JA (2009) Esterification over rare earth oxide and alumina promoted SO_4^{2-}/ZrO_2. Catal Today 148:169–173. https://doi.org/10.1016/j.cattod.2009.03.006
29. Dussadee R, Asama T, Sasikarn N, Wilasinee K, Vichai P, Anusith T, Maythee S, Penjit S (2021) Catalytic behavior of La_2O_3-promoted SO_4^{2-}/ZrO_2 in the simultaneous esterification and transesterification of palm oil. Sci Rep 7:5374–5385. https://doi.org/10.1016/j.egyr.2021.08.166
30. Li C, Zhao Y, Dai B (2012) Study on SO_4^{2-}/ZrO_2-MoO_3 in the integrative transformation of cottonseed oil deodorizing distillate. J Ind Eng Chem 18:520–525. https://doi.org/10.1016/j.jiec.2011.11.058
31. Fan G, Shen M, Zhang Z, Jia F (2009) Preparation, characterization and catalytic properties of $S_2O_8$2-/ZrO_2-CeO_2 solid superacid catalyst. J Rare Earth 27:437–442. https://doi.org/10.1016/S1002-0721(08)60266-5
32. Wang Y, Wang D, Tan M, Jiang B, Zheng J, Tsubaki N, Wu M (2015) Monodispersed Hollow SO3H-functionalized carbon/silica as efficient solid acid catalyst for esterification of oleic acid. Acs Appl Mater Inter 7:26767–26775. https://doi.org/10.1021/acsami.5b08797
33. Pires LHO, De Oliveira AN, Jren OVMRS, Angélica Jr., CEFD Costa, JR Zamian LASD Nascimento GNRF Filho (2014) Esterification of a waste produced from the palm oil industry over 12-tungstophosforic acid supported on kaolin waste and mesoporous materials. Appl Catal B 160–161:122–128. https://doi.org/10.1016/j.apcatb.2014.04.039
34. Veillette M, Giroir-Fendler A, Faucheux N, Heitz M (2017) Esterification of free fatty acids with methanol to biodiesel using heterogeneous catalysts: from model acid oil to microalgae lipids. Chem Eng J 308:101–109. https://doi.org/10.1016/j.cej.2016.07.061
35. Liao Y, Huang X, Liao X, Shi B (2011) Preparation of fibrous sulfated zirconia (SO_4^{2-}/ZrO_2) solid acid catalyst using collagen fiber as the template and its application in esterification. J Mol Catal A 347:46–51. https://doi.org/10.1016/j.molcata.2011.07.009
36. Zalewski DJ, Alerasool S, Doolin PK (1999) Characterization of catalytically active sulfated zirconia. Catal Today 53:419–432. https://doi.org/10.1016/S0920-5861(99)00137-6
37. Jiang K, Tong D, Tang J, Song R, Hu C (2010) The Co-promotion effect of Mo and Nd on the activity and stability of sulfated zirconia-based solid acids in esterification. Appl Catal A 389:46–51. https://doi.org/10.1016/j.apcata.2010.08.062

38. Ropero-Vega JL, Aldana-Pérez A, Gómez R, Niño-Gómez ME (2010) Sulfated titania [TiO_2/SO_4^{2-}]: a very active solid acid catalyst for the esterification of free fatty acids with ethanol. Appl Catal A-Gen 379:24–29. https://doi.org/10.1016/j.apcata.2010.02.020
39. Saravanan K, Tyagi B, Shukla RS, Bajaj HC (2016) Solvent free synthesis of methyl palmitate over sulfated zirconia solid acid catalyst. Fuel 165:298–305. https://doi.org/10.1016/j.fuel.2015.10.043
40. Saravanan K, Tyagi B, Shukla RS, Bajaj HC (2015) Esterification of palmitic acid with methanol over template-assisted mesoporous sulfated zirconia solid acid catalyst. Appl Catal B 172–173:108–115. https://doi.org/10.1016/j.apcatb.2015.02.014
41. Reddy PS, Sudarsanam P, Raju G, Reddy BM (2012) Selective acetylation of glycerol over CeO_2-M and SO_4^{2-}/CeO_2-M (M=ZrO_2 and Al_2O_3) catalysts for synthesis of bioadditives. J Ind Eng Chem 18:648–654. https://doi.org/10.1016/j.jiec.2011.11.063
42. Busca G, Lorenzelli V, Ramis G, Willey RJ (1993) Surface sites on spinel-type and corundum-type metal-oxide powders. Langmuir 9:1492–1499. https://doi.org/10.1021/la00030a012
43. Farhadi S, Panahandehjoo S (2010) Spinel-type zinc aluminate ($ZnAl_2O_4$) nanoparticles prepared by the co-precipitation method: A novel, green and recyclable heterogeneous catalyst for the acetylation of amines, alcohols and phenols under solvent-free conditions. Appl Catal A 382:293–302. https://doi.org/10.1016/j.apcata.2010.05.005
44. Dos Santos VC, Wilson K, Lee AF, Nakagaki S (2015) Physicochemical properties of WO_x/ZrO_2 catalysts for palmitic acid esterification. Appl Catal B 162:75–84. https://doi.org/10.1016/j.apcatb.2014.06.036
45. Li H, Fang Z, Luo J, Yang S (2017) Direct conversion of biomass components to the biofuel methyl levulinate catalyzed by acid-base bifunctional zirconia-zeolites. Appl Catal B 200:182–191. https://doi.org/10.1016/j.apcatb.2016.07.007
46. De Almeida RM, Souza FTC, Júnior MAC, Albuquerque NJA, Meneghetti SMP, Meneghetti MR (2014) Improvements in acidity for TiO_2 and SnO_2 via impregnation with MoO_3 for the esterification of fatty acids. Catal Commun 46:179–182. https://doi.org/10.1016/j.catcom.2013.12.020
47. Nakajima K, Hara M (2012) Amorphous carbon with SO3 groups as a solid bronsted acid catalyst. ACS Catal 2:1296–1304
48. Yan Z, Fan J, Zuo Z, Li Z, Zhang J (2014) NH_3 adsorption on the Lewis and Bronsted acid sites of MoO_3 (010) surface: a cluster DFT study. Appl Sure Sci 288:690–694. https://doi.org/10.1016/j.apsusc.2013.10.105
49. He YY, Ford M, Zhu M, Liu Q, Wu Z, Wachs IE (2016) Influence of catalyst synthesis method on selective catalytic reduction (SCR) of NO by NH_3 with V_2O_5-WO_3/TiO_2 catalysts. Appl Catal B 193:141–150. https://doi.org/10.1016/j.apcatb.2016.04.022
50. Wu YJ, Lin Q, Zhang, GL, Chen L, Guo XW, Liu M (2013) Porous solid superacid SO_4^{2-}/$Fe_{2-x}Zr_xO_3$ fenton catalyst for highly effective oxidation of X-3B under visible light. Ind Eng Chem Res 52:16698–16708. https://doi.org/10.1021/ie402238s
51. M.E. Manríquez, T. López, R. Gómez, J. Navarrete, (2004) Preparation of TiO_2-ZrO_2 mixed oxides with controlled acid-basic properties. J Mol Catal A 220:229–237. https://doi.org/10.1016/j.molcata.2004.06.003
52. Wu T, Wan J, Ma X (2015) Aqueous asymmetric aldol reaction catalyzed by nanomagnetic solid acid SO_4^{2-}/$Zr(OH)_4$-Fe_3O_4. Chinese J Catal 36:425–431. https://doi.org/10.1016/S1872-2067(14)60222-9
53. Witoon T, Permsirivanich T, Kanjanasoontorn N, Akkaraphataworn C, Seubsai A, Faungnawakij K, Warakulwit C, Chareonpanich M, Limtrakul J (2015) Direct synthesis of dimethyl ether from CO_2 hydrogenation over Cu-ZnO-ZrO_2/SO_4^{2-} hybrid catalysts: effects of sulfur-to-zirconia ratios. Catal Sci Technol 5:2347–2357. https://doi.org/10.1039/c4cy01568a
54. Zhao H, Bennici S, Shen J, Auroux A (2010) Nature of surface sites of V_2O_5-TiO_2/SO_4^{2-} catalysts and reactivity in selective oxidation of methanol to dimethoxymethane. J Catal 272:176–189. https://doi.org/10.1016/j.jcat.2010.02.028
55. Duan XL, Yuan DR, Yu FP (2011) Cation distribution in Co-doped $ZnAl_2O_4$ nanoparticles studied by X-ray photoelectron spectroscopy and Al-27 solid-state NMR spectroscopy. Inorg Chem 50:5460–5467. https://doi.org/10.1021/ic200433r
56. Reddy BM, Sreekanth PM, Yamada Y, Kobayashi T (2005) Surface characterization and catalytic activity of sulfate-, molybdate- and tungstate-promoted Al_2O_3-ZrO_2 solid acid catalysts. J Mol Catal A 227:81–89. https://doi.org/10.1016/j.molcata.2004.10.011

57. Ma D, Xin Y, Gao M, Wu J (2014) Fabrication and photocatalytic properties of cationic and anionic S-doped TiO_2 nanofibers by electrospinning. Appl Catal B 147:49–57. https://doi.org/10.1016/j.apcatb.2013.08.004
58. Berrios M, Siles J, Martin M, Martin A (2007) A kinetic study of the esterification of free fatty acids (FFA) in sunflower oil. Fuel 86:2383–2388. https://doi.org/10.1016/j.fuel.2007.02.002